JOURNAL OF PROPULSION AND POWER
Vol. 16, No. 3, May–June 2000

Restricted Shock Separation in Rocket Nozzles

Manuel Frey*
DLR, German Aerospace Research Center, D-74239 Lampoldshausen, Germany
and
Gerald Hagemann†
Dasa, DaimlerChrysler Aerospace, D-81663 Munich, Germany

In overexpanded rocket nozzles the flow separates from the nozzle wall at a certain pressure ratio of wall pressure to ambient pressure. Flow separation and its theoretical prediction have been the subject of several experimental and theoretical studies in the past decades. Two distinctive flow separation phenomena, the free-shock and restricted-shock separation, were observed in experiments with nozzles. Both phenomena are discussed in detail, and the system of recompression shocks and expansion waves is described. For the free-shock case three different shock structures in the plume can occur, namely the regular shock reflection, the Mach disk, or a cap-like shock pattern. The appearance of these different plume patterns is discussed. These shock structures are conserved for the full-flowing, but overexpanded, nozzle. Numerical results obtained for existing rocket nozzles, e.g., Space Shuttle Main Engine or Vulcain, show a qualitative good agreement with experimental photographs. Furthermore, an explanation for the appearance of restricted shock separation, which has been widely unknown up to now, is given, analyzing why and under what conditions it occurs. The type of nozzle contour strongly influences this form of flow separation, and restricted shock separation also occurs in full-scale, thrust-optimized rocket nozzles. Based on the results established for flow separation, an outlook on the generation of side loads is given.

Nomenclature

M = Mach number
p = pressure
x = coordinate parallel to wall
κ = specific heat ratio
Π_c = chamber pressure ratio, $p_c / p_{c,\mathrm{nom}}$
Π_w = wall pressure ratio, p_w / p_a

Subscripts

a = ambient
c = combustion chamber
e = exit plane
nom = nominal
p = plateau downstream of separation
sep = separation
w = wall

Introduction

IN today's launcher vehicles, like the American space shuttle or European Ariane 5, the main engines usually operate from takeoff at sealevel up to high altitudes with very low ambient pressures. In these rocket engines convergent-divergent bell-type nozzles are used to accelerate the hot combustion gases and thus to produce a thrust in the opposite direction. To get an optimum performance over the whole flight trajectory, the nozzles are designed for an intermediate pressure ratio p_c / p_a, at which the exhaust flow is adapted to the ambient pressure. However, this design ambient pressure is chosen high enough to prevent flow separation inside the nozzle during steady-state operation at sea level. Nevertheless, the flow separates from the wall in the divergent part of these nozzles, as long as the chamber pressure p_c has not yet reached its nominal value.

Received 11 August 1998; revision received 29 March 1999; accepted for publication 20 April 1999.

*Research Engineer, Space Propulsion; manuel.frey@dlr.de.
†Project Manager, Space Infrastructure, P.O. Box 801168; gerald.hagemann@ri.dasa.de. Member AIAA.

Flow separation in rocket nozzles is considered undesirable because an asymmetry in the flow separation can cause dangerous lateral forces, the so-called sideloads, which may damage the nozzle. Therefore, flow separation and its theoretical prediction have been and still are the subject of several experimental and theoretical studies.

Two distinctive flow separation phenomena, the free-shock and restricted-shock separation, were observed in experiments with nozzles. In the following, a short literature review on flow separation is given. Then, the restricted shock separation is discussed in detail, including comparisons of numerical and experimental data for different nozzles.

Literature Review

Extensive investigations about flow separation in overexpanded conical nozzles were performed at the Jet Propulsion Laboratory from the late 1940s on, as reported by Summerfield et al.[1] The authors observed flow separation within the nozzle, as soon as the wall pressure at the nozzle exit was lower than about 0.35–0.4 times the ambient pressure, depending on the pressure ratio $p_c / p_{w,e}$. The corresponding formula was soon called the Summerfield criterion. At the separation point the wall pressure quickly rose to a plateau pressure p_p, which is slightly lower than the ambient pressure p_a. The source of this pressure rise was shown to be an oblique shock that originates from the separation point. In the recirculation zone downstream of the separation point, the wall pressure increases slowly from p_p to $p_{w,e}$. The wall pressure in the exit plane $p_{w,e}$ is, in general, not equal to the ambient pressure p_a, but slightly smaller. Nevertheless, the simplification $p_{w,e} = p_a$ is frequently used in the literature. A sketch of the described phenomena is shown in Fig. 1.

Although Summerfield's separation criterion was improved by many authors,[2,3] mainly by including the Mach-number influence, his phenomenological observations were confirmed by numerous tests that were carried out in the following decades, even for different working gases and nozzle contours.[4–7] Once the flow was separated, no reattachment occurred; that is why this standard type of flow separation is called the free-shock separation.

During cold-flow subscale tests for the J-2S engine in the early 1970s,[8] a different kind of separated nozzle flow at strongly overexpanded conditions was observed, which had not been known yet. In this flow regime, which only occurred at pressure ratios

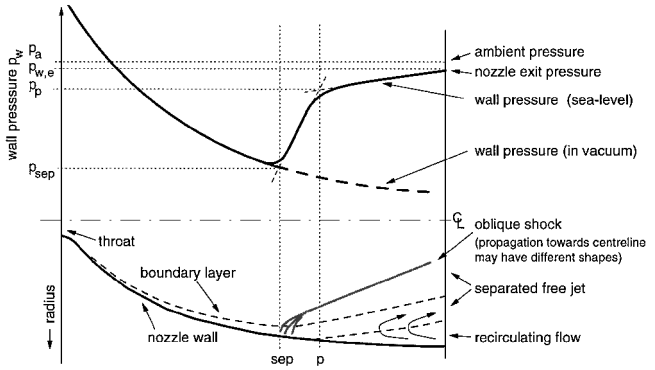

Fig. 1 Free-shock separation in overexpanded rocket nozzles, wall pressure profile, and phenomenology: ——, compression waves/shock, and – – –, boundary/shear-layer edge.

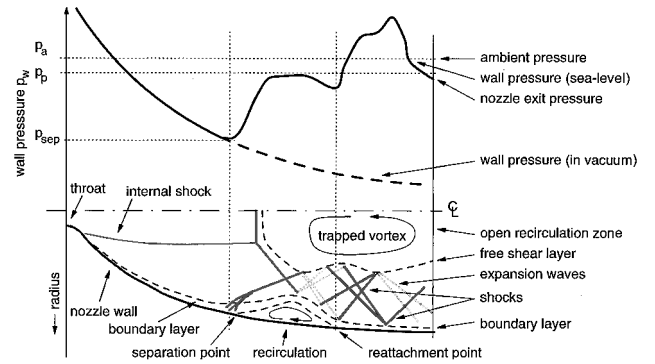

Fig. 2 Restricted-shock separation in overexpanded rocket nozzles, wall pressure profile, and phenomenology: ——, compression waves/shock; · · ·, expansion waves; and – – –, boundary/shear-layer edge.

corresponding to power levels between 34 and 54%, the pressure downstream of the separation point shows an irregular behavior and reaches values even above the ambient pressure. This is attributed to a reattachment of the separated flow to the nozzle wall, inducing shocks and expansion waves, that result in wall pressure peaks with values above ambient pressures. Because of the very short separated region, this flow regime is called restricted-shock separation. A phenomenological sketch of the flowfield and the corresponding wall pressure is shown in Fig. 2.

The observation of reattached flow in the J-2S subscale nozzle was confirmed by numerical simulations by Chen et al.[9] in 1994. In addition, their calculations revealed a trapped vortex behind the central normal shock. Recent cold-flow tests performed by Mattsson et al.[10] showed a similar behavior for a subscale nozzle within a certain pressure range. Together with the J-2S subscale test, these are to the authors' knowledge the only published cases of restricted shock separation.

Up to now, no one has explained why and under what conditions restricted shock separation occurs. In the following, light will be thrown on this question. First, a brief introduction into nozzle design will be given because this seems to have a major influence on the type of flow separation. Then, different flow patterns observed in both experiments and numerical simulations for full- flowing, but overexpanded, nozzles are discussed, followed by an analysis of the restricted-shock separation.

Contour Design of Conventional Rocket Nozzles

For conventional rocket nozzles the following contour design methods are applied:

1) The conical nozzle is the most simple design, with typical divergence angles between 15 and 25 deg, but therefore with high divergence- and-profile losses. This approach is mainly used for solid rocket boosters.

2) The ideal nozzle produces a one-dimensional exhaust flow profile but has a huge length, especially because of the last part of the contour with only minor inclination needed to obtain uniform flow. Because of the low wall slopes, the thrust contribution of this end portion is negligible. Therefore, truncation of the last nozzle portion makes this approach feasible for rocket motors, without significant losses in performance because of the nonuniformity of the flow. As an example, the Viking and the RD-0120 are designed as truncated ideal nozzles.

3) The thrust-optimized nozzle is described next. A variational optimization method based on Lagrange multipliers, which gives the nozzle design for maximum performance at a given length has been proposed by Rao.[11] As a rough approach, the typical length of a Rao-type nozzle is 75–85% of the length of a 15-deg conical nozzle having the same area ratio. Later, Rao[12] also showed that the contour designed with this variational optimization method can be approximated with a skewed parabola, without introducing a significant performance loss. This approach is frequently used for the nozzle design of modern rocket nozzles, e.g., SSME or Vulcain.

In rocket nozzles with conical and thrust-optimized contours, an internal shock is induced in the throat region, where the circular arc forming the nozzle throat turns into the further expansion contour. Further details on this internal shock generation in thrust-optimized rocket nozzles are given in Ref. 13.

Shock Patterns in the Exhaust Plume

In general, the exit wall pressure $p_{w,e}$ of rocket nozzles with operation ranges from sea level to high altitude is chosen high enough to prevent flow separation inside the nozzle. As a consequence, an overexpanded, but attached, nozzle flow is produced at takeoff. At the nozzle exit the lower pressure of the exhaust gases is adapted to the higher ambient pressure by means of an oblique shock. A widespread opinion about the exhaust plume of overexpanded, attached nozzle flows is that there is either a regular reflection of this shock at the centerline or a Mach reflection, resulting in a Mach disk. This is correct for the case of a two-dimensional plane nozzle producing a uniform exit flow as shown in Fig. 3. Which one of these shock patterns will occur mainly depends on the exit pressure ratio p_e/p_a and exit Mach number M_e. Generally, a strong overexpansion and low exit Mach numbers promote the formation of a Mach disk, whereas regular reflection is reached for weaker overexpansion and higher exit Mach numbers.[14] As a rough approximation for air as exhaust gas, regular reflection occurs as soon as the value of the expression $[0.81 \cdot M \cdot (p_e/p_a)^{0.7}]$ exceeds unity (see Ref. 14 for further details).

In a similar, but axisymmetric, form these two shock patterns are observed in conical and truncated ideal nozzles. However, a third shock pattern can exist in thrust-optimized nozzles such as the Vulcain or SSME nozzle. Typical for these nozzles is a flow region near the centerline with highest Mach numbers, also commonly named Kernel,[11] which is bounded by the internal shock. During the startup and shutdown, a cap-like shock pattern is visible in the plume of these nozzles. As examples, Figs. 4 and 5 prove the existence of this specific flow pattern in the plume of both above addressed engines, Vulcain and SSME, respectively.

For the Vulcain engine nozzle during startup, the cap-shock pattern can even be observed for the full-flowing nozzle if the pressure ratio (from chamber pressure p_c to ambient pressure p_a) p_c/p_a does not exceed a critical level of $p_c/p_a \approx 100$–116. Video and motion picture analyses of engine tests performed at DLR revealed that this

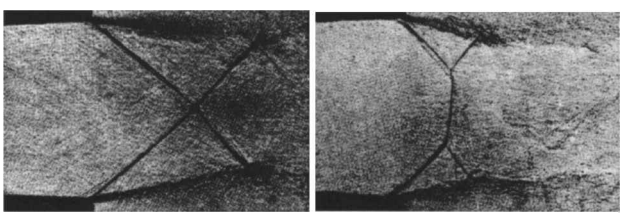

Fig. 3 Shocks in the plume of overexpanded, plane two-dimensional nozzles: regular shock reflection at the centerline (left) and Mach disk (right).[15]

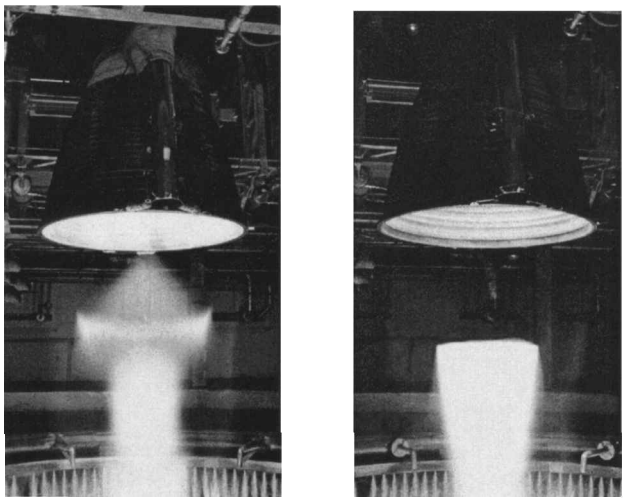

Fig. 4 Vulcain on the P5 test facility at DLR Lampoldshausen: cap-shock pattern (left) and Mach disk (right) (courtesy of SEP).

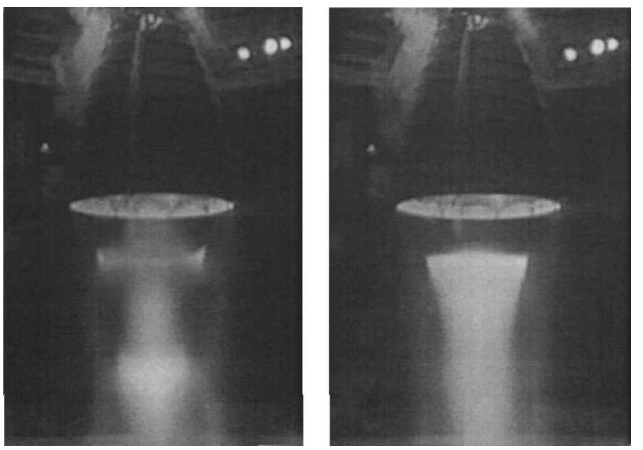

Fig. 5 Hot-firing test of the space shuttle main engine: cap-shock pattern (left) and Mach disk (right) (courtesy of NASA).

plume pattern was observed as a stable and stationary flow pattern even over entire engine test sequences of several minutes. But as soon as the thrust-chamber pressure, respectively the pressure ratio p_c/p_a, exceeded the aforementioned value, the cap-shock pattern was converted into a Mach disk.

For a deeper understanding of this specific plume behavior, numerical flowfield simulations for the Vulcain nozzle were performed by the authors (see Ref. 13 for further details). Boundary conditions assumed in these simplified ideal gas simulations are included in Table 1. The chamber pressure was increased in discrete intervals of 10 bar, until regular reflection was observed in the nozzle plume. These simulations also showed the same plume structures as observed in hot-firing tests, (see Fig. 6). However, the observed switch-over from the cap-shock structure to the Mach disk occurred at higher pressure ratios than in the tests, between $p_c/p_a = 120$ and 130 in the simulation, which might be caused by the simplified ideal gas assumption with constant specific heats.

This specific plume behavior has—based on the authors' knowledge—never been experimentally observed in either conical or truncated ideal nozzles. This implies that the high-Mach-number flow near the centerline limited by the internal shock is responsible for the cap-shock pattern, as it has been only observed in thrust-optimized rocket nozzles, both experimentally and numerically. In fact, a triple point exists, where the internal shock, the small normal shock, and the cone-shaped oblique shock meet (point c in Fig. 7b), indicating a connection between the internal shock and the existence of the cap-shock pattern. Figure 7 emphasizes the essential differences between the cap-shock pattern and the Mach disk. There are three major differences between both plume patterns:

Table 1 Parameters of the Vulcain nozzle, together with data for conical and truncated ideal extension, used for numerical simulations

Parameters	Vulcain data
Chamber stagnation conditions, ideal gas analysis	——
Chamber pressure	100 bar
Chamber temperature	3540 K
Specific heat ratio κ	1.2
Molar mass	13.5 kg/kmole
Geometry area ratio, parabolic contour	45
Geometry area ratio, conical extension (15 deg)	45
Geometry area ratio, truncated ideal contour	38.7

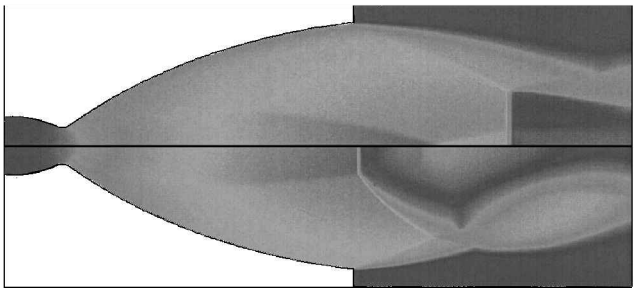

Fig. 6 Numerical simulation of the Vulcain nozzle flow at pressure ratios $p_c/p_a = 130$ (Mach disk, top) and 100 (cap-shock pattern, bottom), respectively.

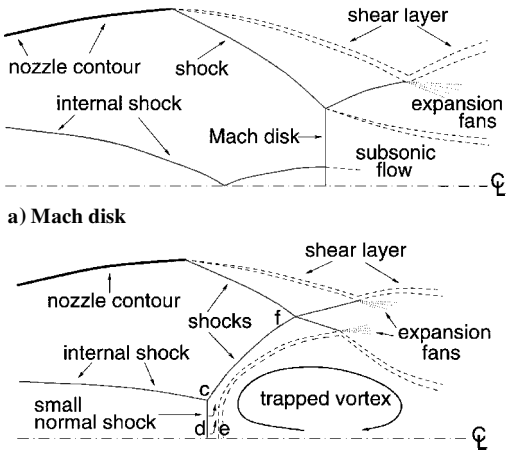

Fig. 7 Shock patterns in the exhaust plume of a thrust-optimized nozzle with internal shock.

1) Across the small normal shock of the cap-shock pattern (points d–e in Fig. 7b), the pressure rises to approximately ambient pressure, whereas downstream of a Mach disk, the pressure is always higher than the ambient.

2) A cap-shock pattern always includes a cone-shaped shock that is inclined away from the centerline (points c–f in Fig. 7b), whereas the oblique shocks occurring upstream of the Mach disk are always inclined toward the axis.

3) A stable vortex is trapped downstream of the small normal shock in the cap-shock pattern, whereas there is no recirculation behind a Mach disk.

The existence of a trapped vortex behind the small normal shock was confirmed in some publications, (see, e.g., Refs. 9 and 10), but other authors have doubted its existence.[16] Up to now, experimental validation for its existence is missing; however, independent numerical simulations, which were performed by Chen et al.,[9] Mattsson et al.,[10] and by the authors,[13] respectively, confirmed the existence of this vortex. One physical explanation for its existence is the curved shock structure upstream of it, thereby generating a certain vorticity. Furthermore, it is driven by an adverse pressure gradient (points a–b in Fig. 8) along the centerline, with the highest pressure in

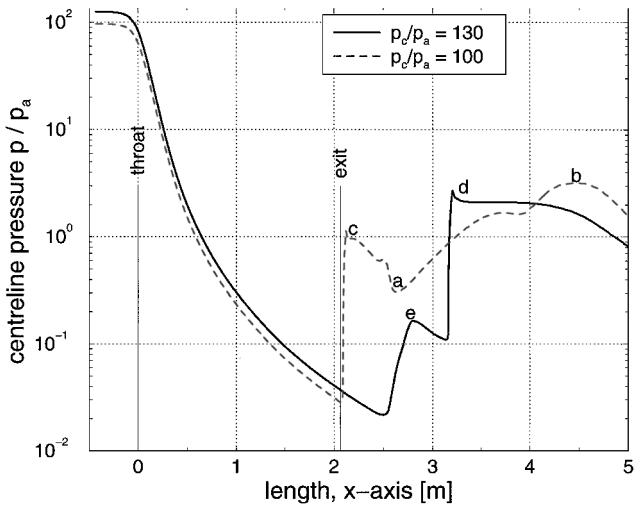

Fig. 8 Centerline pressures for the numerical simulation of the Vulcain nozzle flow at pressure ratios p_c/p_a = 100 and 130, respectively.

the stagnation point closing the trapped vortex further downstream (point b). Also, the vortex seems to be maintained by the shear layer, which is bent around it and therefore additionally supports its existence, as shown in the bottom of Fig. 6.

The calculated centerline pressure profile shown in Fig. 8 also reveals that for the cap-shock structure the pressure behind the small normal shock (point c) is equal to the ambient pressure. In contrast, the Mach disk that was numerically simulated for the higher pressure ratio $p_c/p_a = 130$ results in a pressure downstream of the Mach disk (point d) well above ambient pressure. The small pressure increase upstream of the Mach-disk pressure rise (point e) is caused by the internal shock merging at the centerline.

The transition from cap-shock pattern to the Mach disk occurs as soon as the small normal shock at the centerline in the Kernel, which moves downstream for increasing thrust-chamber pressures, reaches the intersection of the internal shock with the centerline because from that point on there is no higher Mach-number flow near the centerline any more.

The backward transition from Mach disk to the cap-shock pattern during engine throttling or shutdown occurs when the Mach disk, which moves upstream because of the decreasing pressure ratio p_c/p_a, touches this intersection. Obviously, the pressure ratios required for forward and backward transition are not identical, and hence a hysteresis effect should be visible. In fact, this hysteresis effect was clearly observed in hot-firing tests on the P5 test facility and furthermore also in the numerical simulations.[13,14]

Several engine tests revealed that the transition also depends on the thrust-chamber mixture ratio, and thus on the specific heat ratio κ. In these tests, the forward transition occurs for constant chamber pressure p_c but slightly increasing mixture ratio, and hence decreasing average specific heat ratios κ. The distance of the internal shock from the axis decreases with a decreasing κ. Consequently, the intersection point of the internal shock with the centerline moves upstream and finally reaches the small normal shock, which triggers the transition even for constant thrust-chamber pressures.

Based on the video and motion picture analyses of various rocket nozzles performed by the authors, and also based on the various numerical simulations performed with different nozzle types (see, e.g., Refs. 13 and 14), the conclusion can be made that the cap-shock structure only occurs in the plume of thrust-optimized nozzles. Whereas the SSME and Vulcain with induced internal shock showed a clear cap-shock both in experiment as well as in numerical simulations over a certain chamber pressure range, truncated ideal and conical nozzles never showed this kind of plume.

Reattachment of the Separated Flow

In the preceding section shock patterns in the exhaust plume were analyzed for a full-flowing nozzle. If the chamber pressure is lowered, flow separation will occur, and the shock patterns will move into the nozzle. In thrust-optimized nozzles the cap-like form of the shocks will be mainly preserved, whereas in truncated ideal and conical nozzles the Mach disk will occur down to quite low chamber pressures.

As stated before, a cone-shaped oblique shock, which is inclined away from the centerline, exists in thrust-optimized nozzles as a part of the cap-shock pattern. Because of its inclination, this shock deflects the flow away from the centerline in the radial direction. Under the circumstances of flow separation within the nozzle, this means that a momentum toward the nozzle wall is produced. If this momentum is greater than the momentum induced by the separation shock, which turns the boundary layer away from the wall toward the centerline, the flow will be forced to reattach to the wall. Consequently, the probability of restricted shock separation rises if the cone-shaped shock is long and the separation shock is short because, then, the momentum toward the wall is high.

Up to now, also the observation of restricted-shock separation in nozzles has been reported only twice in literature.[8,10] In both cases thrust-optimized subscale nozzles were used, which were fed with cold air. This led to the widespread but erroneous assumption that this type of flow separation could only occur in subscale and cold-flow nozzles.[3] No attention was paid to the nozzle design process. However, many cold-flow subscale experiments with both truncated ideal[5,6,17] and conical nozzles[1,2,6] were performed, where only free-shock separation without reattachment occurred. This is not surprising because truncated ideal nozzles do not feature an internal shock, which could lead to a cap-shock pattern and thus to a radial momentum toward the wall that can make the flow reattach. In conical nozzles the various internal shock reflections at the centerline destroy the high-Mach-number flow, and the Kernel is closed shortly downstream of the throat. Therefore, neither cap-shock pattern nor restricted shock separation can occur in this nozzle family either. As a consequence, the conclusion can be made that the restricted-shock separation phenomenon is triggered by the nozzle contour and not by nozzle size or working gas.

A typical characteristic of restricted-shock separation is the irregular wall pressure profile downstream of the reattachment point, which reaches values higher than the ambient pressure p_a because the flow is attached and supersonic downstream of the reattachment point. In this flow shocks and expansion waves can hit the wall as indicated in Fig. 2, resulting in an unsteady wall pressure.

In the two published cases where restricted-shock separation was observed in experimental setups,[8,10] the separation point is located further downstream than in the free-shock case,[10] as will also be shown next. The reason for this, however, is not a lower separation pressure ratio p_{sep}/p_p, but a much lower value for the plateau pressure p_p. This result is not surprising because the flow downstream of the plateau point is supersonic.

Not only the switch-over from cap-shock pattern to Mach disk, but also the appearance of restricted-shock separation shows a strong hysteresis effect, which was observed in both the J-2S subscale experiments and in Chen et al.'s[9] numerical simulation. According to their results, restricted-shock separation is more likely to occur when the chamber pressure is lowered than when it is increased. This observation is confirmed by additional numerical simulations performed within the frame of this research on the J-2S subscale nozzle.

To understand this hysteresis effect, two points have to be analyzed. First, the position of the small normal shock mainly depends on the pressure ratio p_c/p_a because it increases the pressure to the ambient value as was stated before. On the other hand, there is a hysteresis effect concerning the flow separation process itself,[7] which means that the separation pressure ratio p_{sep}/p_p is higher for increasing pressure ratio $[\delta(p_c/p_a)/\delta t] > 0$ than for a decreasing ratio $[\delta(p_c/p_a)/\delta t] < 0$. By assuming a fixed chamber and ambient pressure, but a slight deviation in the separation pressure ratio p_{sep}/p_p caused by the hysteresis of flow separation, the position of the small normal shock will remain constant, whereas the separation point can vary, as shown in Fig. 9. For $[\delta(p_c/p_a)/\delta t] > 0$, x_{sep} will be smaller than for $[\delta(p_c/p_a)/\delta t] < 0$, which also means that for a decreasing

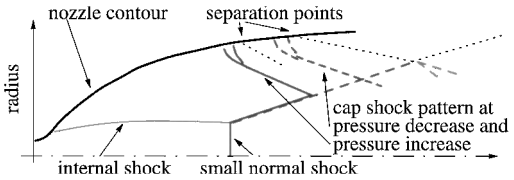

Fig. 9 Hysteresis of flow separation and its influence on reattachment: Increasing chamber pressure produces free-shock separation (left), whereas decreasing chamber pressure results in restricted shock separation (right).

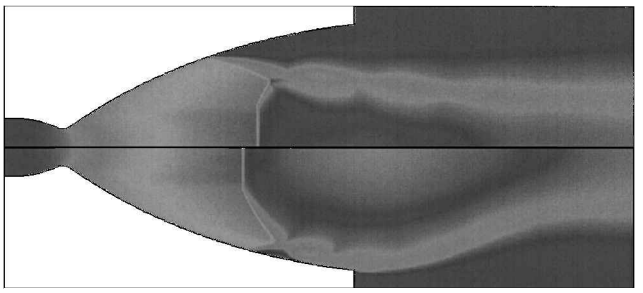

Fig. 10 Numerical simulation of the Vulcain nozzle flow at a pressure ratio p_c/p_a = 40 with free-shock separation (top) and restricted-shock separation (bottom), respectively.

pressure ratio the cone-shaped shock that produces a momentum toward the wall is longer and the separation shock is shorter than in the case of decreasing pressure ratio. As a consequence, the net momentum toward the wall, which can cause reattachment, will be greater if $[\delta(p_c/p_a)/\delta t] < 0$ and the probability of restricted-shock separation will therefore increase.

Restricted-Shock Separation in Full-Scale Rocket Nozzles

Up to now, restricted-shock separation was believed not to occur in full-scale nozzles, although there is no physical reason, why this phenomenon should be limited to subscale cold-flow nozzles. To investigate whether restricted-shock separation may occur also in hot-gas full-scale nozzles, numerical simulations for various full-scale nozzles with different contour designs were performed in a first step. During startup, reattachment of the flow could be observed only in the simulated SSME nozzle. Additionally, both nozzles, the Vulcain and SSME, showed restricted-shock separation over a certain range of pressure ratios when the chamber pressure was lowered. The two flowfield structures for the Vulcain nozzle at one fixed pressure ratio $p_c/p_a = 40$ are shown in Fig. 10. The upper part shows the free-shock separation that occurs when the chamber pressure is increased, whereas the lower part illustrates the restricted-shock separation that occurs if $[\delta(p_c/p_a)/\delta t] < 0$. Corresponding wall pressures are shown in Fig. 11 (dashed line), clearly illustrating the irregular wall pressure profile with values above ambient pressure for the restricted-shock separation. Additionally, downstream displacement of the separation point is obvious for the restricted-shock separation.

As a next step, two nozzle extensions for the Vulcain engine were designed for a further comparison, a conical and a truncated ideal one. Design data are included in Table 1. In contrast to the original parabolic nozzle extension, clear Mach disks and hence no restricted-shock separation were observed in both the conical and the truncated ideal nozzle, as shown in Figs. 12 and 13, respectively.

The question rises whether restricted-shock separation really exists in the full-scale Vulcain or SSME nozzle. Therefore, analyses of full-scale tests of the Vulcain nozzle were recently performed, (see Ref. 18 for further details). A comparison of experimentally measured wall pressures and computed values for an axial location close to the nozzle exit is given in Fig. 14. Experimental data were measured in five different positions in the circumferential direction,

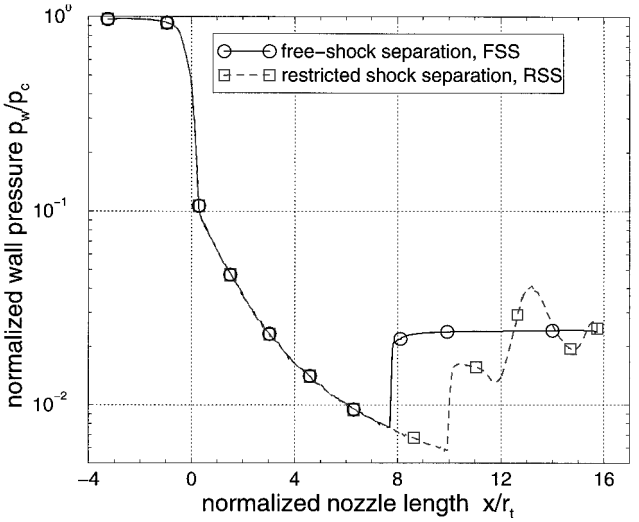

Fig. 11 Wall pressures for the numerical simulation of the Vulcain nozzle flow at a pressure ratio p_c/p_a = 40 for: ——, increasing, and – – –, decreasing chamber pressure.

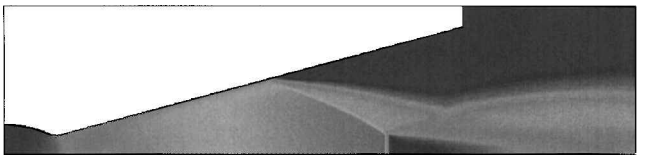

Fig. 12 Numerical simulation of a conical nozzle flow at a pressure ratio p_c/p_a = 40, with free-shock separation, chamber geometry, and area ratio as Vulcain nozzle.

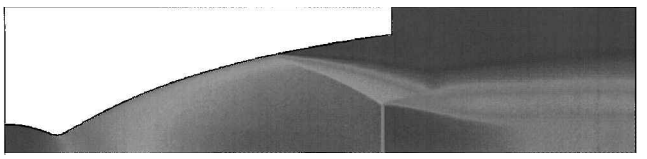

Fig. 13 Numerical simulation of a truncated ideal nozzle flow at a pressure ratio p_c/p_a = 60 with free-shock separation, chamber geometry, and performance values as Vulcain nozzle.

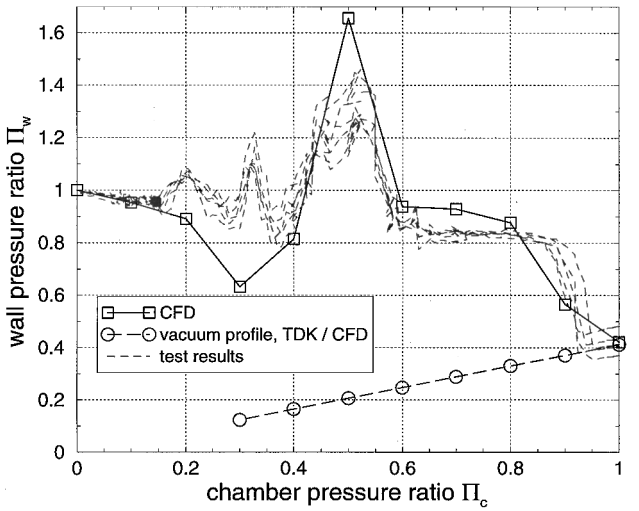

Fig. 14 Numerical and experimental wall pressure data of the Vulcain nozzle as a function of the chamber pressure ratio Π_c and wall pressure transducer located near nozzle exit.[18]

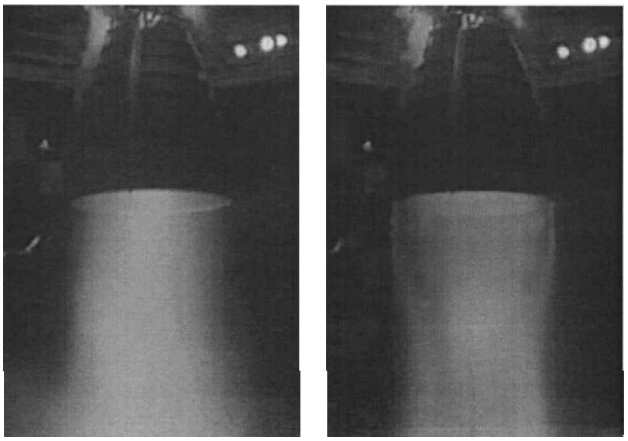

Fig. 15 Hot-firing test of the space shuttle main engine: flow pattern during startup with flow separation far inside the nozzle (courtesy of NASA).

which are all included in Fig. 14, but not individually distinguished. For certain chamber pressure ratios the wall pressure shows an irregular behavior by approaching values above ambient pressures. The calculated wall pressures of the aforementioned numerical simulations show an astonishing similarity with the experimental values.

Besides the wall pressure data, visual plume analyses of the startup and shutdown process in both engines nozzle, SSME and Vulcain, showed a shear layer originating from the nozzle exit very close to the nozzle wall for such low chamber pressures that neither cap shocks nor a Mach disk were visible in the plume. It seems as if the flow were attached to the wall in the exit plane—probably because of the restricted-shock separation pattern because in case of free-shock separation the plume only covers a small fraction of the nozzle exit plane near the centerline. As an example, Fig. 10 illustrates the position of the shear layer relative to the nozzle exit plane for both separation patterns. Figure 15 shows two images taken during startup of the SSME with flow separation far inside the nozzle. The different locations of the shear layer emanating from the nozzle are obvious. The left image shows the radiating shear layer far away from the nozzle wall, as expected for the free-shock separation. In contrast, the right image, taken only milliseconds later, seems to show the restricted-shock separation: the shear layer is attached to the nozzle wall, and near the centerline a radiating core can be observed indicating subsonic flow with high temperatures. Both phenomena show close analogies to the restricted-shock separation.

Generation of Side-Loads—An Outlook

In the following, a nozzle is considered where at startup first free-shock separation and later restricted-shock separation occurs. If the transition from the one to the other separation pattern requires a certain time, a phase might exist, during which one side of the nozzle experiences a free-shock separation while at the other side the flow reattaches. Because the separation point is located further downstream in the restricted-shock case and the wall pressure behaviors are totally different between the two cases, there would be severe lateral forces acting on the nozzle. The main characteristic of these side forces would be their high value and the short period of time they occur.

In the same nozzle a second side-load peak could be expected during startup as soon as the reattachment point reaches the nozzle exit and ambient air can flow into the previously closed recirculation zone. In this moment the restricted-shock separation would be converted into a free-shock one with the same characteristics (strong, but short lateral force) as just described. Two distinct and short side-load peaks are well visible in the measurements published in Ref. 10, and their occurrence corresponds to a change in separation pattern as proved by wall pressure measurements. A comparison between the side-loads that are caused by a change in separation pattern and the side-load behavior of both the Vulcain engine and the SSME shows astonishing similarities. As expected, the side-load behavior of truncated ideal nozzles shows a much smoother slope without significant peaks and of much lower value,[19] which supports the aforementioned theory.

Therefore, future side-load investigations will have to include analyses of the type of separation pattern, in addition to other possible influences, e.g., pressure oscillations at the separation point and in the separated region, or a coupling of fluid-dynamic behavior with the structure.

Conclusion

The restricted-shock separation phenomenon, observed in experiments with subscale nozzles and also in recent numerical calculations but not at all understood up to now, has been considered in more detail in this paper. Its appearance is closely linked with the cap-like shock pattern observed in the plume of thrust-optimized rocket nozzles that feature a Kernel with highest Mach numbers near the centerline and a limiting internal shock induced in the throat region at the joining of the circular arc with the further expansion contour. A cone-shaped shock associated with the cap-shock pattern introduces a radial momentum toward the wall, which may force the reattachment of the exhaust flow downstream of the separation point. For truncated ideal nozzles, where no internal shock is induced, neither a cap-like shock pattern in the plume nor restricted-shock separation have been observed in experiments or numerical simulations. In spite of their internal shock, the same observation also holds for conical nozzles, as they do not have the flow structure of thrust-optimized nozzles inside the nozzle with the high-Mach-number region near the centerline.

Visual plume analyses of the SSME and Vulcain engine during hot-firing tests showed a flow structure at the nozzle exit, which can be explained by restricted-shock separation for lower chamber pressures. Also, their typical side-load behavior shows astonishing similarities with lateral forces potentially induced by a sudden change from free- to restricted-shock separation.

Acknowledgment

The authors acknowledge Société Européenne de Propulsion for permission to publish Vulcain data. The Vulcain engine was developed by SEP as the main contractor in the frame of an ESA program, with the Centre National d'Etudes Spatiales acting as a delegate of ESA for the execution of this program.

References

[1] Summerfield, M., Foster, C., and Swan, W., "Flow Separation in Overexpanded Supersonic Exhaust Nozzles," *Jet Propulsion*, Vol. 24, No. 9, 1954, pp. 319–321.

[2] Arens, M., and Spiegler, E., "Shock Induced Boundary Layer Separation in Overexpanded Conical Exhaust Nozzles," *AIAA Journal*, Vol. 1, No. 3, 1963, pp. 578–581.

[3] Schmucker, R., "Strömungsvorgänge beim Betrieb Überexpandierter Düsen Chemischer Raketentriebwerke (Flow Processes in Overexpanded Nozzles of Chemical Rocket Engines)," Technical Univ., Rept. TB-7, -10, -14, Munich, July 1973.

[4] Campbell, C. E., and Farley, J. M., "Performance of Several Conical Convergent-Divergent Rocket-Type Exhaust Nozzles," NASA TN D-467, May 1960.

[5] Farley, J. M., and Campbell, C. E., "Performance of Several Method-of-Characteristics Exhaust Nozzles," NASA TN D-293, April 1960.

[6] Lawrence, R. A., "Symmetrical and Unsymmetrical Flow Separation in Supersonic Nozzles," Ph.D. Dissertation, Inst. of Technology, Southern Methodist Univ., Dallas, TX, April 1967.

[7] Sunley, H. L. G., and Ferriman, D. L. C., "Jet Separation in Conical Nozzles," *Journal of the Royal Aeronautical Society*, Vol. 68, No. 12, 1964, pp. 808–817.

[8] Nave, L. H., and Coffey, G. A., "Sea Level Side Loads in High-Area-Ratio Rocket Engines," AIAA Paper 73-1284, July 1973.

[9] Chen, C. L., Chakravarthy, S. R., and Hung, C. M., "Numerical Investigation of Separated Nozzle Flows," *AIAA Journal*, Vol. 32, No. 9, 1994, pp. 1836–1843.

[10] Mattsson, J., Högman, U., and Torngren, L., "A Sub-Scale Test Programme on Investigation of Flow Separation and Side-Loads in Rocket Nozzles," *Proceedings of the 3rd European Symposium on Aerothermodynamics of Space Vehicles*, ESA-ESTEC, Noordwijk, The Netherlands, 1998, pp. 373–378.

[11]Rao, G. V. R., "Exhaust Nozzle Contours for Optimum Thrust," *Jet Propulsion*, Vol. 28, No. 6, 1958, pp. 377–382.
[12]Rao, G. V. R., "Approximation of Optimum Thrust Nozzle Contours," *ARS Journal*, Vol. 30, No. 6, 1960, p. 561.
[13]Frey, M., and Hagemann, G., "Status of Flow Separation Prediction in Rocket Nozzles," AIAA Paper 98-3619, July 1998.
[14]Frey, M., "Shock Patterns in the Exhaust Plume of Rocket Nozzles," *Proceedings of the 3rd European Symposium on Aerothermodynamics of Space Vehicles*, ESA-ESTEC, Noordwijk, The Netherlands, 1998, pp. 395–403.
[15]Shapiro, A. H., *Compressible Fluid Flow*, Wiley, New York, 1953, pp. 556, 557.
[16]Hadjadj, A., "Analyse Physique et Simulation Numerique des Ecoulements Compressibles—Application Aux Tuyeres de Propulseurs (Physical Analysis and Numerical Simulation of Compressible Flows—Application to Rocket Nozzles)," Ph.D. Dissertation, Faculté des Sciences, Univ. of Rouen, France, Jan. 1997.
[17]Girard, S., and Alziary de Roquefort, T., "Study of Flow Separation in Overexpanded Rocket Nozzles," 4th French-Russian-Italian-Uzbek Workshop, Marseille, France, July 1997.
[18]Terhardt, M., Hagemann, G., and Frey, M., "Flow Separation and Side-Load Behaviour of the Vulcain Engine," AIAA Paper 99-2763, June 1999.
[19]Dumnov, G. E., "Unsteady Side-Loads Acting on the Nozzle with Developed Separation Zone," AIAA Paper 96-3220, July 1996.